Trapping and binding of an arbitrary number of cylindrical particles in an in-plane electromagnetic field

Tomasz M. Grzegorczyk, Brandon A. Kemp, and Jin Au Kong

Research Laboratory of Electronics, Massachusetts Institute of Technology, Cambridge, Massachusetts 02139

Received January 9, 2006; revised March 1, 2006; accepted March 16, 2006; posted April 6, 2006 (Doc. ID 66668)

The Mie theory and the Foldy–Lax multiple-scattering equations are applied to compute the scattered field of an arbitrary number of infinite dielectric cylinders of arbitrary size, subject to in-plane incidences. The Maxwell stress tensor is then used to compute the force on each cylinder. Trapping and binding forces are studied as a function of particle size, number, permittivity, and separation. Finally, the formulation is applied to a system of 20 particles, and the results show clear similarities with known experimental reports. The formulation presented here extends the capabilities of modeling particle interaction and optical matter beyond the simple cases of the Rayleigh regime and two-particle systems.

OCIS codes: 290.4210, 260.2110, 020.7010.

1. INTRODUCTION

The manipulation of small dielectric particles, typically dielectric spheres, by electromagnetic waves was first demonstrated in Ref. 1 and was immediately followed by important experimental observations such as optical levitation[2] and single-beam trapping.[3] In such experiments, the exerting force on the particles is due to the transfer of momentum from the incident electromagnetic wave to the particles, as was already predicted by James C. Maxwell. Levitation and trapping are associated with two different physical origins: Levitation is due to the scattering force of the impinging electromagnetic wave, and trapping is due to the gradient of the electric field intensity acting on small particles. These two new effects found applications in systems where minute particles needed to be displaced without damage.[4] Optical binding was later reported[5,6] as a third manifestation of the optical forces generated within a system of particles submitted to an electromagnetic excitation. Optical binding, which can become a dominant effect in the near field of the particles and can dictate their motion, can be understood as a secondary trapping effect, due not to the sole incident field but to the scattered field from all the particles in the system. Both trapping and binding have been recently experimentally verified on a collection of spherical polystyrene beads submitted to two different types of incidence,[7,8] and a new trapping regime based on binding forces has been reported in Ref. 9.

The theoretical understanding of such experiments requires the computation of the force via either the Maxwell stress tensor[10,11] or the Lorentz force on bound currents and charges (Ref. 12 and references herein). In both cases, the methods require the knowledge of the total electric and magnetic field around or within the particles due to the incident wave and the scattered waves from all the particles in the system. With an increasing number of randomly positioned particles, the computation of the total field quickly becomes nontrivial so that first theoretical considerations have been limited to considering only special cases where approximations could be used. Typically, a widely studied situation involves a single particle in a Rayleigh regime: it has been shown that the force can be split into the gradient force and scattering force,[13–16] respectively referring to the force due to the gradient of the field intensity and to the force due to the momentum of the electromagnetic wave. However, the Rayleigh model approximates the scattered field of the particle by a dipole radiation and therefore has to be used with caution for larger particles or when multiple particles are considered in a close proximity. The scattering from large spherical particles can be directly obtained from the Mie theory; some researchers have used different approaches such as the discrete dipole approximation[17] (DDA) to study particles in the presence of a ground plane[18] or the multiple-multipole method to study cylindrical circular and elliptical objects.[19] However, the computation of the force on a system of multiple particles has not received much attention yet, despite some work on a particle in a complex environment such as a rough surface[20,21] and on a system of two particles still in the Rayleigh regime[22] or using the DDA.[23] The advantage of the approach used in Ref. 23 is the inherent advantage of DDA, namely, the flexibility of studying particles of arbitrary shapes and permittivities, but the disadvantages of the DDA are that large particles require important computer resources. This is particularly true when the fields need to be computed in the close proximity of the particle boundary, where a large number of dipoles have to be used in order to reduce the effects of surface discretization.

In the present paper, we present an exact theoretical model based on Mie theory to compute the force on an arbitrary number of dielectric particles under plane-wave incidences. For the purpose of simplicity, we limit ourselves to infinite dielectric cylinders and in-plane incidences (i.e., with all the wave vectors perpendicular to the axes of the cylinders) with the electric field parallel to the

axis of the cylinders, but the theory is directly generalizable to oblique incidences and spherical particles as well. The interactions between the particles are computed using the Foldy–Lax exact multiple-scattering equations, yielding the expansion coefficients of the total field in the cylindrical coordinate system $(\hat{\boldsymbol{\rho}}, \hat{\boldsymbol{\phi}}, \hat{\mathbf{z}})$. The advantage of the method is the ability to model an arbitrary number of particles of arbitrary sizes, without additional approximation other than the mode truncation in the cylindrical wave expansion. The disadvantages are that the particles are required to be of a canonical shape (cylinders in our case) and of identical permittivity. Since the number of particles as well as the number of plane-wave incidences can be arbitrary, both trapping and binding phenomena can be predicted, as we shall illustrate hereafter. We should note that the limitations of in-plane incidence and identical radius (which we shall use later) are easily lifted. In addition, the case of an electric field perpendicular to the axis of the cylinders is not discussed here but could be studied in a very similar manner.

2. CYLINDRICAL WAVE EXPANSION AND FOLDY–LAX APPROACH TO MULTIPLE SCATTERING

The problem we are considering is expressed as follows: a total of L infinite cylinders with their axes parallel to $\hat{\mathbf{z}}$ are located at positions (x_ℓ, y_ℓ) $(\ell = 1, \ldots, L)$. For the sake of simplicity, all the cylinders are assumed to be identical, of radius a, real relative permittivity ϵ_c, wavenumber k_c, and nonmagnetic. A plane wave with electric field $\mathbf{E}_{\text{inc}}(\boldsymbol{\rho}) = \hat{\mathbf{z}} E_0 e^{i\mathbf{k}\cdot\boldsymbol{\rho}}$ is incident onto the system with $\mathbf{k} = \hat{\mathbf{k}} k = \hat{\mathbf{x}} k_x + \hat{\mathbf{y}} k_y$, where a bold symbol denotes a vector and a hat denotes a vector of norm 1. It is already well known that such incidence, along with the associated magnetic field, can be decomposed onto a cylindrical coordinate system as[24]

$$\mathbf{E}_{\text{inc}}(\boldsymbol{\rho}) = \hat{\mathbf{z}} E_0 e^{i\mathbf{k}\cdot\boldsymbol{\rho}} = \sum_{\mathsf{n}=-\infty}^{+\infty} a_{\mathsf{n}} Rg\mathbf{N}_{\mathsf{n}}(k, \boldsymbol{\rho}), \tag{1a}$$

$$\mathbf{H}_{\text{inc}}(\boldsymbol{\rho}) = -\frac{\hat{\mathbf{z}} \times \hat{\mathbf{k}}}{|\hat{\mathbf{z}} \times \hat{\mathbf{k}}|} \frac{E_0}{\eta_0} e^{i\mathbf{k}\cdot\boldsymbol{\rho}}, \tag{1b}$$

where $a_{\mathsf{n}} = E_0 \mathrm{i}^{\mathsf{n}} e^{-\mathrm{i}\mathsf{n}\phi_i}/k$. The scattered field in the region outside the cylinder is decomposed in a similar fashion as

$$\mathbf{E}_{\text{scat}}(\boldsymbol{\rho}) = \sum_{\mathsf{n}=-\infty}^{+\infty} a_{\mathsf{n}}^s \mathbf{N}_{\mathsf{n}}(k, \boldsymbol{\rho}), \tag{2a}$$

$$\mathbf{H}_{\text{scat}}(\boldsymbol{\rho}) = \frac{1}{\mathrm{i}\eta} \sum_{\mathsf{n}=-\infty}^{+\infty} a_{\mathsf{n}}^s \mathbf{M}_{\mathsf{n}}(k, \boldsymbol{\rho}), \tag{2b}$$

where η is the impedance of the background medium. In Eqs. (1) and (2),

$$\mathbf{M}_{\mathsf{n}}(k, \boldsymbol{\rho}) = \hat{\rho} \frac{\mathrm{i}\mathsf{n}}{\boldsymbol{\rho}} H_{\mathsf{n}}^{(1)}(k\rho) e^{\mathrm{i}\mathsf{n}\phi} - \hat{\phi} k H_{\mathsf{n}}^{(1)\prime}(k\rho) e^{\mathrm{i}\mathsf{n}\phi}, \tag{3a}$$

$$\mathbf{N}_{\mathsf{n}}(k, \boldsymbol{\rho}) = \hat{\mathbf{z}} k N_{\mathsf{n}}^{(1)}(k\rho) e^{\mathrm{i}\mathsf{n}\phi}, \tag{3b}$$

where the prime denotes a derivative with respect to the argument and where the Hankel functions are replaced by the Bessel function for $Rg\mathbf{M}_{\mathsf{n}}$ and $Rg\mathbf{N}_{\mathsf{n}}$. Note that in Eqs. (2) the coefficients a_{n}^s are unknown and are solved for upon applying the boundary condition on the total tangential electric and magnetic fields at the boundary of the cylinder. Before this is done, the fields inside the cylinder also need to be expressed as in Eqs. (2) with another set of unknown coefficients. However, since we shall use in this paper the approach based on the Maxwell stress tensor, the computation of the force on the cylinder due to the incident field requires the knowledge of the field outside the cylinder only; hence we do not write the field inside for brevity. When multiple particles are present, Eqs. (2) need to be generalized so that the scattered field of a given particle includes the effects from the incident field and from the scattered field of all the other particles, including all interactions. The self-consistent formulation proposed by Foldy[25] and Lax[26] is used here and can be written as[24]

$$\mathbf{E}^{ex(q)}(\boldsymbol{\rho}) = \mathbf{E}_{\text{inc}}(\boldsymbol{\rho}) + \sum_{\substack{\ell=1 \\ l \neq q}}^{L} \mathbf{E}_{\text{scat}}^{(\ell)}(\boldsymbol{\rho}). \tag{4}$$

Equation (4) states that the final exciting field of particle q is equal to the incident wave plus the scattered waves to particle q from all the other particles ℓ except q itself. As a generalization of Eqs. (2), $\mathbf{E}_{\text{scat}}^{(q)}(\boldsymbol{\rho})$ is written as

$$\mathbf{E}_{\text{scat}}^{(q)}(\boldsymbol{\rho}) = \sum_{\mathsf{n}=-\infty}^{+\infty} a_{\mathsf{n}}^{s(q)} \mathbf{N}_{\mathsf{n}}(k, \boldsymbol{\rho} - \boldsymbol{\rho}_q), \tag{5}$$

where the cylindrical functions $\mathbf{N}_{\mathsf{n}}$ have to be evaluated at translated origins for each particle q located at $\boldsymbol{\rho}_q = (x_q, y_q)$. The coefficients $a_{\mathsf{n}}^{s(q)}$ are the generalized version of a_{n}^s and reduce to a_{n}^s in the case of a single particle. Their expression is obtained from

$$a_{\mathsf{n}}^{s(q)} = T_{\mathsf{n}} w_{\mathsf{n}}^{(q)}, \tag{6}$$

where T_{n} is the known T coefficient of a cylinder for the given polarization,

$$T_{\mathsf{n}} = \frac{k_c}{k} \frac{J_{\mathsf{n}}(k_c a)}{H_{\mathsf{n}}^{(1)}(ka)} B_{\mathsf{n}} - \frac{J_{\mathsf{n}}(ka)}{H_{\mathsf{n}}^{(1)}(ka)}, \tag{7a}$$

$$B_{\mathsf{n}} = \frac{2\mathrm{i}k}{\pi a k_c} [k H_{\mathsf{n}}^{(1)\prime}(ka) J_{\mathsf{n}}(k_c a) - k_c J_{\mathsf{n}}'(k_c a) H_{\mathsf{n}}^{(1)}(ka)]^{-1}, \tag{7b}$$

and where $w_{\mathsf{n}}^{(q)}$ are solved from

$$w_{\mathsf{n}}^{(q)} = e^{i\mathbf{k}\cdot\boldsymbol{\rho}_q} a_{\mathsf{n}} + \sum_{\mathsf{n}'=-\infty}^{+\infty} \sum_{\substack{\ell=1 \\ l \neq q}}^{L} H_{\mathsf{n}-\mathsf{n}'}^{(1)}(k|\boldsymbol{\rho}_l - \boldsymbol{\rho}_q|) e^{-\mathrm{i}(\mathsf{n}-\mathsf{n}')\phi_{lq}} T_{\mathsf{n}'} w_{\mathsf{n}'}^{(\ell)}, \tag{8}$$

with $\phi_{\ell q}$ being the angle between the $\hat{\mathbf{x}}$ axis and the vector joining the centers or particles (ℓ) and (q). Equation (8) has been obtained upon applying the translational

theorem of the Hankel function to each individual particle:

$$H_{\mathsf{n}'}^{(1)}(k|\boldsymbol{\rho}_\ell-\boldsymbol{\rho}_p|)e^{\mathrm{i}\mathsf{n}'\phi_{lp}}=\sum_{\mathsf{n}=-\infty}^{+\infty}J_{\mathsf{n}}(k|\boldsymbol{\rho}_\ell-\boldsymbol{\rho}_q|)e^{\mathrm{i}\mathsf{n}\phi_{lq}}\times H_{\mathsf{n}-\mathsf{n}'}^{(1)}(k|\boldsymbol{\rho}_p-\boldsymbol{\rho}_q|)e^{-\mathrm{i}(\mathsf{n}-\mathsf{n}')\phi_{pq}}. \quad (9)$$

In practice, the infinite sums are truncated at $N=\max(\mathsf{n})$ $(\Sigma_{-\infty}^{+\infty}\rightarrow\Sigma_{-N}^{+N})$, where N has to be properly chosen as a function of the number of particles in the system, their size, permittivity, and separation, in order to achieve good convergence (values of N are specified in each case hereafter). The solution of the system of Eq. (8) requires the inversion of a square matrix of dimensions $L\times(2N+1)=21L$ for $N=10$. For our purpose, a direct Gauss inversion is used, but more efficient algorithms can be implemented to improve the computation efficiency of the calculation. It should be noted that such matrix size is significantly smaller than the one obtained from a DDA method applied to particles of similar properties. Hence, losing the ability of modeling arbitrary shapes and permittivities, we gain a considerable saving in computer memory and computational time.

Once the $w_{\mathsf{n}}^{(q)}$ coefficients are solved for, $a_{\mathsf{n}}^{s(q)}$ are computed from Eq. (6), and $\mathbf{E}_{\mathrm{scat}}^{(q)}(\boldsymbol{\rho})$ is obtained from Eq. (5). Finally, the total scattered field is expressed as

$$\mathbf{E}_{\mathrm{scat}}(\boldsymbol{\rho})=\sum_{q=1}^{L}\mathbf{E}_{\mathrm{scat}}^{(q)}(\boldsymbol{\rho}). \quad (10)$$

The interior fields are obtained in a similar manner but are not required for the computation of the force on the cylinders in our case.

Knowing the scattered field, and therefore the total fields $(\mathbf{E},\mathbf{H})$ in the region outside all cylinders, we compute the time-averaged Lorentz force from the Maxwell's stress tensor as[10,27]

$$\mathbf{F}=\oint_C \mathrm{d}\ell\left[\frac{\epsilon}{2}\mathrm{Re}\{(\mathbf{E}\cdot\hat{\mathbf{n}})\mathbf{E}^*\}+\frac{\mu}{2}\mathrm{Re}\{(\mathbf{H}\cdot\hat{\mathbf{n}})\hat{\mathbf{H}}^*\}-\frac{\epsilon}{4}(\mathbf{E}\cdot\mathbf{E}^*)\hat{\mathbf{n}}-\frac{\mu}{4}(\mathbf{H}\cdot\mathbf{H}^*)\hat{\mathbf{n}}\right]. \quad (11)$$

In Eq. (11), Re{ } denotes the real-part operator, $\hat{\mathbf{n}}=\hat{\boldsymbol{\rho}}$ is the normal vector to the surface of the cylinder, and the closed contour C surrounds the particle from the outside, thus requiring the knowledge of the fields outside the particle only. In this case, the permittivity ϵ and permeability μ are those of the background medium. Equation (11) has already been extensively used in the literature but often applied to small particles. In such cases, gradient and scattering forces can be separated, and a series of approximations can be used to simplify Eq. (11) into expressions with direct physical interpretations. However, in the case of large particles, or when many closely packed particles are considered, no systematic approximation of Eq. (11) can be used. As we shall see hereafter, the results of the force on large particles or on many particles do not always follow the intuition built from the study of small particles.

The validation of the previous equations has been performed by comparing the predicted total field scattered by multiple particles with that obtained by the commercial package CST MICROWAVE STUDIO. The comparison has been done with a number of particles, ranging from one to five, submitted to one, two, and three incident plane waves. In all cases, the fields (E_z,H_x,H_y) have been monitored and verified to agree well, both inside and outside the dielectric cylinders. In addition, the force has been compared with the one obtained by the method presented in Ref. 12 in the way shown in Refs. 28 and 29, where bound currents and charges are used within the volume of the particle. The agreement between the two calculation methods has been found to be excellent in all the situations studied hereafter. A noticeable advantage of the Maxwell stress tensor approach, however, is that it requires fewer integration points, since the force is expressed as a line integral instead of a surface integral. On the other hand, the method of bound currents and charges has the advantage of computing the local force density within the particle, which is not accessible from the Maxwell stress approach.

3. EVIDENCE OF THE TRAPPING FORCE

Trapping of particles has been experimentally verified in Refs. 6 and 7 with a set of three incident Gaussian beams. The corresponding conclusions are here confirmed theoretically on a simplified system of cylindrical particles submitted to three plane waves of identical amplitude $E_0=1$ (V/m) propagating in the (xy) plane with angles $\{\pi/2,7\pi/6,11\pi/6\}$ (rad). The three incident plane waves have a similar wavelength in free space of $\lambda=546$ nm, and the particles are polystyrene cylinders of permittivity $\epsilon_c=2.56\epsilon_0$ embedded in water $(\epsilon=1.69\epsilon_0)$. The radius of the particles used in Ref. 7 is 1 μm, which is not a constraint in our case since size is not a limitation. However, the traps created by the three in-plane incident waves are smaller than 1 μm, as can be seen from the background pattern in Fig. 1, and therefore 1 μm particles would feel the effect of multiple traps. To keep the particle size of the same order as the traps, we resort to particles of radii $a=0.15\lambda=81.9$ nm and $a=0.3\lambda=163.8$ nm.

The trapping force on a single particle is shown in Fig. 1 where the background field pattern shows the interference of the three incident plane waves (only a relevant portion of the (xy) plane is shown, since the pattern is periodic in both directions) and the arrows show the force acting on the particle as it sweeps the (xy) plane. The arrows in Fig. 1 show both the relative magnitude and direction of the force, where the starting point of each arrow corresponds to the location of the center of the cylinder at which the computation is performed. It can immediately be seen that the trapping ability of the incident pattern is significantly different for the two different sizes of particles: The high field intensity at $(x,y)=(0,0)$ is a point of stable equilibrium for $a=0.15\lambda$, while it is a point of unstable equilibrium for $a=0.3\lambda$. It should be noted that a similar behavior was found in Ref. 30 for a particle in the Rayleigh regime $(a\ll\lambda/20)$ as a function of its refractive index.

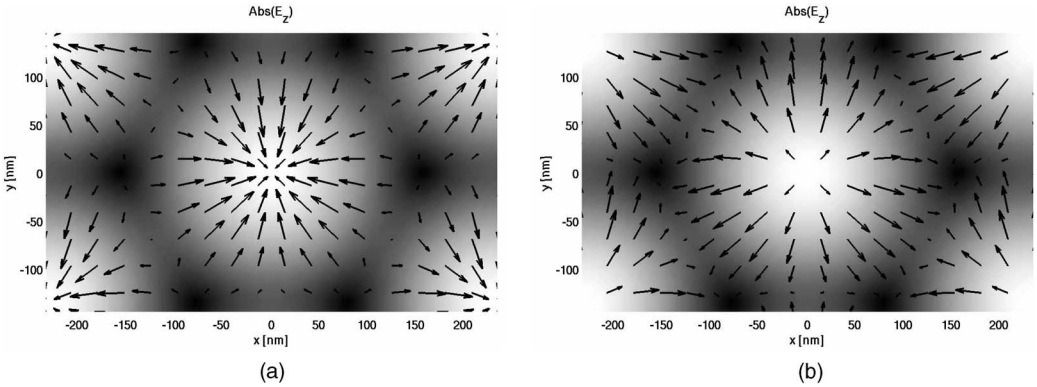

Fig. 1. Force (represented by the black arrows) on a single cylinder due to the interference of three plane waves (represented by the background pattern) of identical amplitude $E_0=1$ (V/m), wavelength $\lambda=546$ nm, and incident angles $\{\pi/2, 7\pi/6, 11\pi/6\}$ (rad). Other parameters are $\epsilon_c=2.56\epsilon_0$, $\epsilon=1.69\epsilon_0$, $N=5$, and the radius a of the cylinder is as indicated. The background pattern shows the absolute value of the electric field on a scale from 0 (V/m) (black) to 3 (V/m) (white) (a) $a=0.15\lambda$, (b) $a=0.3\lambda$.

In Fig. 1(a), the force pattern is seen to closely obey a gradient law, which can be expected for small particles. In fact, calculations have been performed for a series of sizes smaller than $a=0.15\lambda$, and all yielded a similar force pattern. The drastic difference with the pattern of Fig. 1(b) indicates the limit of the gradient approximation. With these properties (size and permittivity contrast), the particle is already slightly larger than a trap and feels the influence of the periodic repetition of the high field intensities. Interestingly, calculations with particles of sizes $a=0.5\lambda$ reveal a force pattern very similar to the one of Fig. 1(a), while particles of $a=0.75\lambda$ yield a pattern similar to Fig. 1(b). In both cases, however, the particles are very large compared with the trapping sites, and a simple gradient law is not expected to remain valid. Finally, it is worth mentioning that, for large particles, vortices are formed in the regions of low intensities: The particles are attracted toward these regions and are trapped following a spiral motion before coming to rest.

The results of Fig. 1 have been obtained with 11 cylindrical modes ($N=5$), which we have confirmed to be sufficient to yield an error of less than 1% compared with our reference computed with 81 modes ($N=40$).

4. EVIDENCE OF BINDING FORCE

Unlike the trapping force, which is immediately felt by a single particle in a properly arranged incident-field configuration, binding forces require multiple particles. In principle, binding forces arise as soon as two particles are present: the scattered field of the first one modifies the incident field on the second one, thus modifying the force that would have been felt by the second particle if it had been alone. In practice, however, the perturbation of the incident field by the scattered field is often weak, and binding forces are easier to measure when a large number of particles scatter together.[7]

In theoretical calculations such as we present here, however, two particles are sufficient to show the binding effect. The configuration, originally studied in Ref. 23 on very small particles ($a\simeq\lambda/60$), is depicted in Fig. 2: two particles are aligned in the $\hat{\mathbf{x}}$ direction and submitted to a single incident plane wave propagating in the $\hat{\mathbf{y}}$ direction. If the two particles were isolated, only a force in the $\hat{\mathbf{y}}$ direction (due to the transfer or momentum from the electromagnetic wave to the particle) would be measured. Hence, any force in the $\hat{\mathbf{x}}$ direction is due to interaction effects, associated with binding phenomena.

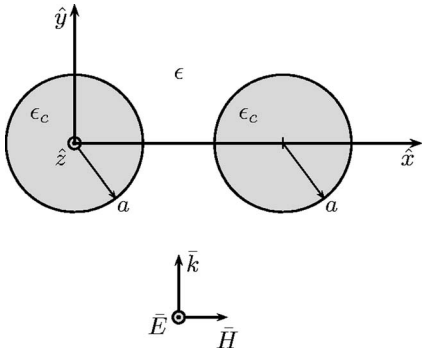

Fig. 2. Two infinite cylinders of radius a and permittivity ϵ_c are embedded in a background medium of permittivity $\epsilon=1.69\epsilon_0$ and subject to an incident field propagating in the $\hat{\mathbf{y}}$ direction as indicated.

Figure 3 shows the $\hat{\mathbf{x}}$ directed force on the right-hand particle in Fig. 2 as function of relative distance and particle size. Since the system is symmetric, the force on the left-hand particle is immediately obtained by symmetry. It can be seen first that the force is oscillatory as a function of the distance between the two particles. This observation generalizes the result already presented in Ref. 23 for very small particles. Second, it is seen that the strength of the force does not depend on the particle size in a trivial way: Although the strength is generally larger with the larger particle, the strength on the particle with $a=0.3\lambda$ is smaller than on the particle with $a=0.15\lambda$. We attribute this effect to the size of the particle compared with the trapping site. As has been mentioned already, a particle with $a=0.15\lambda$ is approximately the same size as the trap, while a particle with $a=0.3\lambda$ is slightly larger already (i.e., the particle feels a nonnegligible influence from the neighboring traps), and a particle with $a=0.5\lambda$ is influenced by many traps. The same effect that dictates the difference in the trapping force patterns of Fig. 1 dictates here the difference between the binding forces. Furthermore, we have confirmed that for particles smaller than the traps, the binding force diminishes with the size

of the particle. Such result could be confirmed by an analysis in the Rayleigh regime but is outside the scope of this paper. The effect of the permittivity of the cylinders on the binding force is illustrated in Fig. 4. As expected, the larger the permittivity contrast between the particle and the background, the stronger the binding. This effect is here confirmed far from the Rayleigh regime and can be directly understood from the Born approximation: the scattered field is directly proportional to $(\epsilon_c - \epsilon)$ and is therefore reduced in a low-permittivity contrast system.

Finally, we analyze the amplitude of the force exerted on the right-hand particle as a function of the number of particles on the left. The results for one particle are identical to the ones presented in Fig. 4 with the corresponding parameters, while the cases of two and four particles are illustrated in the insets of Fig. 5. The computation is performed here with $N=20$ to ensure good convergence of the fields even for closely packed cylinders as in the four-cylinder case. Two interesting conclusions can be drawn from these results. First, the binding force is stronger within the system of three particles than in the system of two particles. This directly justifies the experimental verification that binding phenomena become measurable when multiple particles are scattering together.[7] Second,

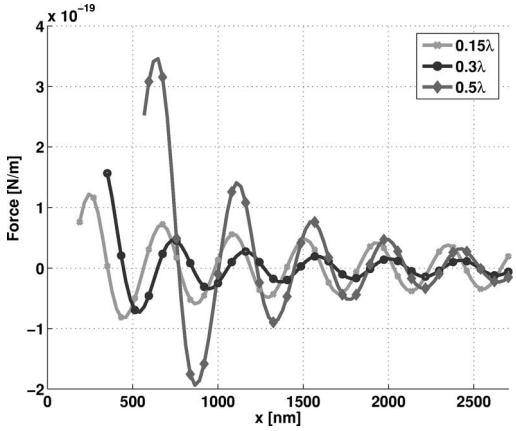

Fig. 3. Force in the $\hat{\mathbf{x}}$ direction for the configuration of Fig. 2 as a function of the relative distance between particles. The parameters are $\lambda=546$ nm, $\epsilon_c=2.56\epsilon_0$, $\epsilon=1.69\epsilon_0$, $N=10$, and radius a as indicated in the labels.

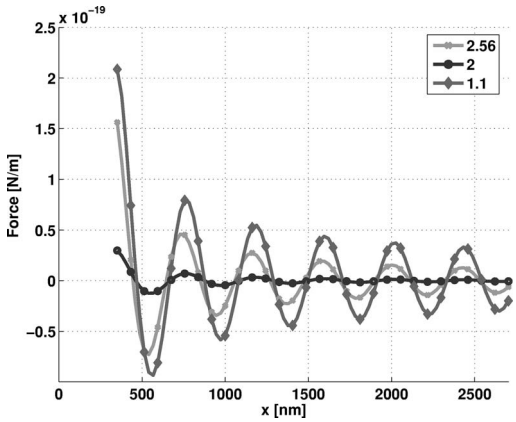

Fig. 4. Force in the $\hat{\mathbf{x}}$ direction for the configuration of Fig. 2 as a function of the relative distance between particles. The parameters are $\lambda=546$ nm, $\epsilon=1.69\epsilon_0$, $a=0.3\lambda$, and $N=10$. The relative permittivity of the cylinders is as indicated in the labels.

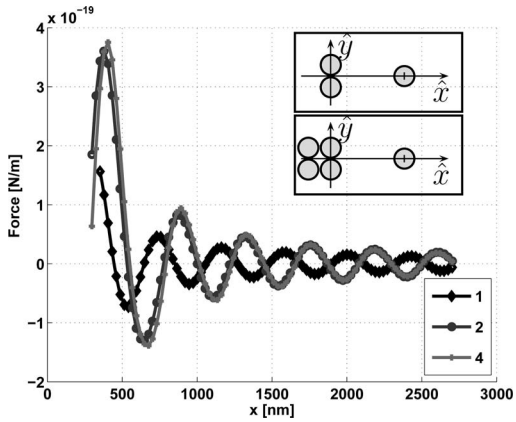

Fig. 5. Force in the $\hat{\mathbf{x}}$ direction for varying number of cylinders on the left (the force and the positions are for the particle on the right). The case of one cylinder corresponds to Fig. 2, the cases of two and four cylinders correspond to the situations shown in the insets. The positions of the fixed cylinders are $(x,y)=(0,\pm 170\text{ nm})$ and $(x,y)=\{(-170\text{ nm},\pm 170\text{ nm}),(0,\pm 170\text{ nm})\}$ in the cases of two and four particles, respectively. The parameters are $\lambda=546$ nm, $\epsilon_c=2.56\epsilon_0$, $\epsilon=1.69\epsilon_0$, $a=0.3\lambda$, and $N=20$.

the binding force is almost identical in the three-particle system and the five-particle system. Hence, this result puts a limitation on the previous conclusion, which is related to the incident field: in the configuration studied here, the scattered fields from two and four particles on the left along the $\hat{\mathbf{x}}$ axis are almost identical. This can be directly understood from a generalization of the Mie theory, which indicates that a large particle has a strong forward scattering and low side scattering. The clusters of two and four particles behave in some sense like a single large particle, having different forward-scattering fields and similar side-scattering fields. Hence, the similarity in the binding force would obviously not hold for an $\hat{\mathbf{x}}$-directed incidence, in which case the particle on the right would be in the forward-scattering region of the clusters and would be affected differently by their scattered fields.

5. RANDOM ARRANGEMENT OF 20 PARTICLES

Within the limitation of in-plane incident waves, we reproduce here part of the experimental conclusions of Ref. 7. Toward this purpose, we return to the case of three plane-wave incidences like those shown in Fig. 1, where all the parameters are as indicated in the caption of the figure. The size of the cylinders is taken to be $a=0.15\lambda$ since we have seen in Fig. 1(a) that the incident interference pattern yields good traps. Within a region of space of $(5a\times 5a)$, we randomly position 20 particles and compute the force on each due to the incident field and the scattered field from all the particles in the system. The position of each particle is then adjusted in space by an amount proportional to the force acting on it. Mathematically, if we denote by (x_ℓ^i, y_ℓ^i) and $(f_{x\ell}^i, f_{y\ell}^i)$ the position and force on particle ℓ at iteration i, respectively, the updated positions at iteration $(i+1)$ are obtained from

$$x_l^{i+1} = x_l^i + \alpha f_{xl}^i, \tag{12a}$$

$$y_l^{i+1} = y_l^i + \alpha f_{yl}^i, \tag{12b}$$

where α is arbitrarily chosen such that the particles are not moved too much or too little between the first and second iterations (we typically tolerate a motion within a fraction of the particle radius). At the new set of positions, the forces acting on each particle are computed again, and the process is reiterated until the correction terms on the positions are negligible (typically less than 1% of the current position). It should be emphasized that the motion of the particles resulting from this iterative process is not strictly derived from the equations of motions of mechanics but is merely a visual tool to estimate the evolution of the particles as a function of the forces acting on them when strong damping is present as in the case of a water background.

The experiment with 20 particles was repeated multiple times, each time with a different set of initial positions. An example of initial positions is given in Table 1 and illustrated in Fig. 6(a). Because of the large number of particles in the relatively small constrained surface, the particles are often closely packed over single trapping sites and may compete for a site until an equilibrium is reached. The equilibrium is attained either when the particles rearrange themselves to occupy separate traps, as shown in Fig. 6(b) (with the final positions given in Table 1) or when the total field is such that the effect of neighboring traps on a conglomerate of particles produces no force, as shown close to the origin in Fig. 6(d). In both final positions, it should also be noted that the particles do not always settle in regions of high field intensity, where the traps are predicted to be the strongest for a single particle [see Fig. 1(a)]. This is a direct manifestation of the binding forces: The scattered field by all the particles, including all their interactions, modifies the incident-field pattern and thus modifies the location of the traps. The background pattern shown in Fig. 6(b), representing the incident field only, therefore only serves as a reference to see where the traps should have been if the scattered field between the particles had been ignored. Obviously, the final positions do not correspond to the traps due to the incident field, and therefore the gradient force approximation used in the modeling of small particles cannot be used in this case. Figure 6(c) shows the same case as Fig. 6(b) with the background pattern corresponding to the total field instead of the incident field only. Interestingly, it is seen that the particles come to rest in regions of high total field intensity, indicating that for such size the gradient force due to the total field is dominant.

Finally, we have confirmed that if the dielectric contrast between the background medium and the particles is very low (typically, $|\epsilon_c - \epsilon| \simeq 0.1$), the traps due to the incident field on a single particle are still located in the high-field regions as in Fig. 1(a), and their strength is significantly increased. The immediate consequence is that when a set of 20 such particles are randomly positioned within an area of $(5a \times 5a)$ the particles evolve to almost exactly occupy the positions of high field intensities due to the incident waves only, similar to what has been experimentally reported in Refs. 7 and 31. This indicates not

Table 1. Initial Positions (x_i, y_i) and Final Positions (x_f, y_f) of 20 Particles in a Three-Plane-Wave Interference Pattern[a]

x_i (nm)	y_i (nm)	x_f (nm)	y_f (nm)
−148.91	−59.30	−200.08	−120.94
−377.76	−388.95	−410.69	−533.34
296.79	−380.12	179.12	−356.27
30.74	−335.74	−7.45	−486.75
−106.53	396.91	18.50	454.02
286.33	−85.47	398.75	16.19
278.84	301.18	219.68	374.49
−272.76	179.49	−427.16	245.14
−276.50	362.89	−219.12	346.56
279.25	91.55	204.00	111.49
−287.76	−231.91	−388.75	−230.97
42.83	17.06	−5.79	−2.15
70.09	231.64	−7.01	235.09
−310.92	3.13	−409.60	19.53
−151.11	−349.56	−198.72	−402.18
10.59	−162.72	2.95	−247.57
−101.12	118.56	−206.37	118.08
388.51	−224.98	416.51	−199.41
168.19	−235.86	193.02	−125.97
141.00	397.59	249.79	633.45

[a]The corresponding positions are shown in Figs. 6(a) and 6(b).

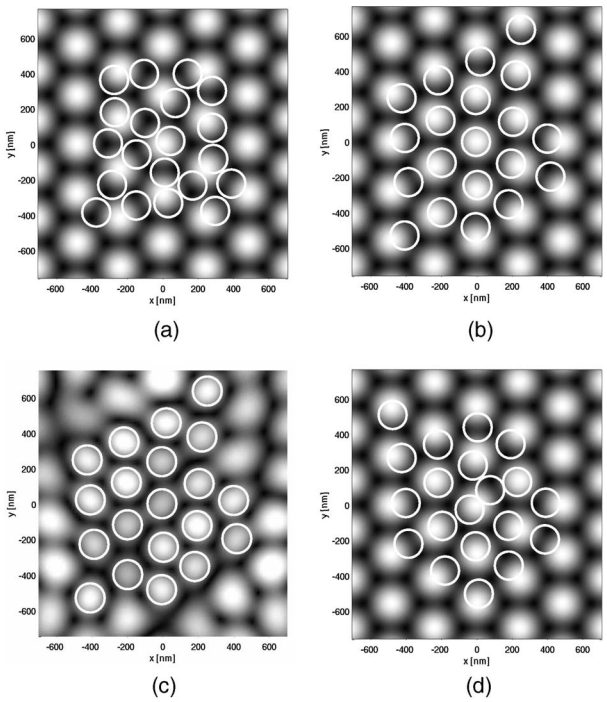

Fig. 6. Positions of 20 dielectric cylinders and field distributions (shown in the background) for various cases: (a) random initial position in a three-plane-wave interference pattern (incident field shown); (b) organized final position due to trapping and binding forces (incident field shown); (c) same as case (b) but with the total field shown; (d) organized final position corresponding to another set of initial positions different from that in case (a). In all cases, the parameters are $\lambda = 546$ nm, $\epsilon_c = 256\epsilon_0$, $\epsilon = 169\epsilon_0$, $a = 0.15\lambda$, and $N = 10$. The background patterns show the absolute value of the electric field (either incident or total field) on a scale from 0 (black) to 3 V/m (white).

only the good efficiency of the traps but also that the scattering is weak and does not perturb the incident waves significantly. For this type of dielectric contrast, a Born approximation can be used to compute the field in the system and confirm these conclusions.

6. CONCLUSIONS

We have demonstrated in this paper that both trapping and binding forces in a complex arrangement of particles can be predicted without approximations on particle size, permittivity, or separation. The theoretical model, based on an extension of Mie theory to cylindrical particles combined with the Foldy–Lax multiple-scattering equations and the Maxwell stress tensor, has been shown to predict some recent experimental results reasonably well with limited requirements on computer memory. Such modeling capability represents a step forward in the understanding of optical tweezers, optical matter, and other systems where large particles are manipulated by radiation pressure.

ACKNOWLEDGMENTS

It is a pleasure to acknowledge many stimulating discussions with J.-M. Fournier. This work is sponsored by the Department of the U.S. Air Force under Air Force contract FA8721-05-C-0002 and by the Chinese National Foundation under contracts 60371010 and 60531020. Opinions, interpretations, conclusions, and recommendations are those of the author and are not necessarily endorsed by the U. S. Government.

Corresponding author T. M. Grzegorczyk can be reached by e-mail at tomasz@mit.edu.

REFERENCES

1. A. Ashkin, "Acceleration and trapping of particles by radiation pressure," Phys. Rev. Lett. **24**, 156–159 (1970).
2. A. Ashkin and J. M. Dziedzic, "Optical levitation by radiation pressure," Appl. Phys. Lett. **19**, 283–285 (1971).
3. A. Ashkin and J. M. Dziedzic, "Optical levitation in high vacuum," Appl. Phys. Lett. **28**, 333–335 (1976).
4. A. Ashkin, "Applications of laser radiation pressure," Science **210**, 1081–1088 (1980).
5. M. M. Burns, J.-M. Fournier, and J. A. Golovchenko, "Optical binding," Phys. Rev. Lett. **63**, 1233–1236 (1989).
6. M. M. Burns, J.-M. Fournier, and J. A. Golovchenko, "Optical matter: crystallization and binding in intense optical fields," Science **249**, 749–754 (1990).
7. J.-M. Fournier, G. Boer, G. Delacrétaz, P. Jacquot, J. Rohner, and R. Salathé, "Building optical matter with binding and trapping forces," in Proc. SPIE **5514**, 309–317 (2004).
8. A. Casaburi, G. Pesce, P. Zemánek, and A. Sasso, "Two- and three-beam interferometric optical tweezers," Opt. Commun. **251**, 393–404 (2005).
9. T. M. Grzegorczyk, B. A. Kemp, and J. A. Kong, "Stable optical trapping based on optical binding forces," Phys. Rev. Lett. **96**, 113903 (2006).
10. J. Stratton, *Electromagnetic Theory* (McGraw-Hill, 1941).
11. J. A. Kong, *Electromagnetic Wave Theory* (EMW, 2000).
12. A. R. Zakharian, M. Mansuripur, and J. V. Moloney, "Radiation pressure and the distribution of electromagnetic force in dielectric media," Opt. Express **13**, 2321–2336 (2005).
13. A. Ashkin, "Trapping of atoms by resonance radiation pressure," Phys. Rev. Lett. **40**, 729–732 (1978).
14. J. P. Gordon, "Radiation forces and momenta in dielectric media," Phys. Rev. A **8**, 14–21 (1973).
15. P. C. Chaumet and M. Nieto-Vesperinas, "Time-averaged total force on a dipolar sphere in an electromagnetic field," Opt. Lett. **25**, 1065–1067 (2001).
16. J. R. Arias-González and M. Nieto-Vesperinas, "Optical forces on small particles: attractive and repulsive nature and plasmon-resonance conditions," J. Opt. Soc. Am. A **20**, 1201–1209 (2003).
17. E. M. Purcell and C. R. Pennypacker, "Scattering and absorption of light by nonspherical dielectric grains," Astrophys. J. **186**, 705–714 (1973).
18. P. C. Chaumet and M. Nieto-Vesperinas, "Coupled dipole method determination of the electromagnetic force on a particle over a flat dielectric substrate," Phys. Rev. B **61**, 14119–14127 (2000).
19. C. Rockstuhl and H. P. Herzig, "Rigorous diffraction theory applied to the analysis of the optical force on elliptical nano- and micro-cylinders," J. Opt. A, Pure Appl. Opt. **6**, 921–931 (2004).
20. A. Madrazo and M. Nieto-Vesperinas, "Scattering of electromagnetic waves from a cylinder in front of a conducting plane," J. Opt. Soc. Am. A **12**, 1298–1309 (1995).
21. A. Madrazo and M. Nieto-Vesperinas, "Surface structure and polariton interactions in the scattering of electromagnetic waves from a cylinder in front of a conducting grating: theory for the reflection photon scanning tunneling microscope," J. Opt. Soc. Am. A **13**, 785–795 (1996).
22. F. Depasse and J.-M. Vigoureux, "Optical binding force between two Rayleigh particles," J. Phys. D **27**, 914–919 (1994).
23. P. C. Chaumet and M. Nieto-Vesperinas, "Optical binding of particles with or without the presence of a flat dielectric surface," Phys. Rev. B **64**, 035422 (2001).
24. L. Tsang, J. Kong, K. Ding, and C. Ao, *Scattering of Electromagnetic Waves: Numerical Simulations* (Wiley, 2000).
25. L. L. Foldy, "The multiple scattering of waves," Phys. Rev. **67**, 107–119 (1945).
26. M. Lax, "Multiple scattering of waves. II. The effective field in dense systems," Phys. Rev. **85**, 261–269 (1952).
27. M. Lester and M. Nieto-Vesperinas, "Optical forces on microparticles in an evanescent laser field," Opt. Lett. **24**, 936–938 (1999).
28. B. A. Kemp, T. M. Grzegorczyk, and J. A. Kong, "*Ab initio* study of the radiation pressure on dielectric and magnetic media," Opt. Express **13**, 9280–9291 (2005).
29. B. A. Kemp, T. M. Grzegorczyk, and J. A. Kong, "Lorentz force on dielectric and magnetic particles," J. Electromagn. Waves Appl. **20**, 827–839 (2006).
30. P. Zemánek, V. Karásek, and A. Sasso, "Optical forces acting on Rayleigh particle placed into interference field," Opt. Commun. **240**, 401–415 (2004).
31. J.-M. Fournier, J. Rohner, P. Jacquot, R. Johann, S. Mias, and R. Salathé, "Assembling mesoscopic particles by various optical schemes," in Proc. SPIE **5930**, 238–247 (2005).